# Relating Structure and Chemical Composition with Lewis Acidity in Zeolites: A Spectroscopic Study with Probe Molecules

**Gabriela Catana,[†] David Baetens,[†] Tim Mommaerts,[†] Robert A. Schoonheydt,[†] and Bert M. Weckhuysen*[,†,‡]**

*Centrum voor Oppervlaktechemie en Katalyse, Departement Interfasechemie, K. U. Leuven, Kardinaal Mercierlaan 92, B-3001 Heverlee, Belgium, and Departement Anorganische Chemie en Katalyse, Debye Instituut, Universiteit Utrecht, Sorbonnelaan 16, P.O. Box 80083, 3508 TB Utrecht, The Netherlands*

*Received: August 24, 2000; In Final Form: February 2, 2001*

FTIR and EPR of adsorbed probe molecules were used to study Lewis acid sites in FAU and MFI zeolites with different nonframework Al content. Infrared spectra of adsorbed CO at low temperatures give information about all types of sites. The absorption bands were assigned to CO fixed on Brönsted sites, cations, and true Lewis acid sites with different strengths. The frequency shifts and the relative intensities of these peaks were correlated with the structure type and the nonframework Al amount. In contrast, EPR of adsorbed NO is probing only the sites strong enough to quench the orbital magnetic moment of NO molecule. However, the method can provide an estimation of the strength of the detected Lewis acid sites, via the $g_{zz}$ parameter. A correlation was established between the amount of nonframework Al and the spin concentrations of adsorbed NO. These absolute concentrations are lower than the expected number of Lewis acid sites. Several methods were proposed for creating Lewis acid sites in a controlled way. Among them, alumination and mild steaming were the most efficient, leading to well-distributed nonframework Al species, which act as strong Lewis acid sites. Despite its high nonframework Al content, the severely steamed zeolite Y has weak sites, only partially accessible for probe molecules, such as CO and NO.

## Introduction

One major issue in research on zeolites is the characterization of Brönsted and Lewis acid centers. Brönsted acid sites (BAS) are assigned to bridging hydroxyl groups and various techniques have successfully been applied to study their structure, concentration and strength.[1] Lewis acid sites (LAS) are essentially electron acceptor centers and they can be cations or different aluminum species located in defect centers, the so-called true Lewis sites.

The origins of Lewis acidity in zeolites are diverse and depend on the structure and chemical composition of the material under investigation. While cations in zeolites are well characterized,[2−6] the structure of true Lewis sites is still controversial. Some authors associate LAS with trigonal Al atoms formed as a result of zeolite dehydroxylation by thermal treatment.[7] Other research groups have proposed $Al^{3+}$-species, or various other nonframework species ($AlO^+$, $Al(OH)^{2+}$, $Al(OH)_2^+$, $Al(OH)_3$, AlO(OH), $Al_2O_3$, etc.), leached from the zeolite framework during chemical or thermal treatment.[8,9,10] The exact nature of these species is, however, still unknown.

Among the different techniques used to study surface acidity, spectroscopy of adsorbed probe molecules has been extensively applied. Numerous papers and reviews have been published mainly about the Fourier transform infrared spectroscopy (FTIR) and probe molecules, such as pyridine, ammonia and acetonitriles.[1,11] With the availability of the in-situ cells for low-temperature measurements, many studies were devoted to adsorbed diatomic molecules like CO and $N_2$, which are suitable for investigating both Brönsted and Lewis acidity.[12−21] The electric field of an electron deficient site is able to quench the orbital magnetic moment of an adsorbed molecule. If, as a consequence, the molecule exhibits a magnetic moment, like in the case of the nitric oxide (NO), one may use this interaction to identify and characterize the Lewis acid sites in zeolites with electron paramagnetic resonance (EPR).[22−28]

In this paper, we present a spectroscopic study of Lewis acidity in zeolites as a function of the structure type, chemical composition and nonframework aluminum content. The Lewis acid sites were identified by FTIR of adsorbed CO at low temperatures and by EPR of adsorbed NO. In both cases, the spectroscopic results can be related with the strength and the number of Lewis acid sites. Catalytic studies have shown that the activity of Lewis acid sites depends on both the structure type and chemical composition of zeolites.[29] Therefore, we have investigated a series of zeolite samples differing in structure type (FAU and MFI) and aluminum content (Si/Al ratio between 3.6 and 40). Moreover, the type of nonframework aluminum species and their distribution seem to be important parameters, too. Therefore, alumination and dealumination processes of zeolite Y were conducted in order to create nonframework species in a controlled way.

## Experimental Section

**1. Materials.** The investigated samples are presented in Table 1. The CBV series of faujasite (FAU) and pentasil (MFI) zeolites were obtained from PQ and used as received. The MFI samples are all ZSM-5 zeolites in their ammonium form: CBV3020 (Si/Al = 15), CBV5020 (Si/Al = 25), and CBV8020 (Si/Al = 40).

* To whom correspondence should be addressed. E-mail address: bert.weckhuysen@agr.kuleuven.ac.be

[†] Centrum voor Oppervlaktechemie en Katalyse.

[‡] Departement Anorganische Chemie en Katalyse.

10.1021/jp003091v CCC: $20.00 
Published on Web 05/03/2001

**TABLE 1: Total Al, Framework Al, and Nonframework Al Content of the Samples Investigated in This Work**

| sample/code | total Al[a] (mmol Al/g) | framework Al[b] (mmol Al/g) | nonframework Al (mmol Al/g) |
|---|---|---|---|
| H−Y/Y | 2.94 | 2.94 | 0 |
| USY/CBV712 | 2.58 | 1.43 | 1.15 |
| USY/CBV720 | 1.15 | 1 | 0.15 |
| USY/CBV780 | 0.44 | 0.33 | 0.11 |
| steamed H−Y/SY1 | 2.94 | 0.99 | 1.94 |
| steamed H−Y/SY2 | 2.94 | 2.36 | 0.57 |
| Al−H−Y/AlY | 3.20 | 2.94 | 0.26 |
| Al−H−Y/$Al_{ex}$Y | 3.93 | 2.94 | 0.99 |
| La−H−Y/LaY | 2.94 | 2.94 | 0.31[c] |
| H−ZSM-5/CBV3020 | 0.95 | 0.78 | 0.17 |
| H−ZSM-5/CBV5020 | 0.645 | 0.61 | 0.035 |
| H−ZSM-5/CBV8020 | 0.415 | 0.4 | 0.015 |

[a] Determined with chemical analysis. [b] Determined with $^{27}$Al MAS NMR. [c] $La^{3+}$ amount (mmol/g).

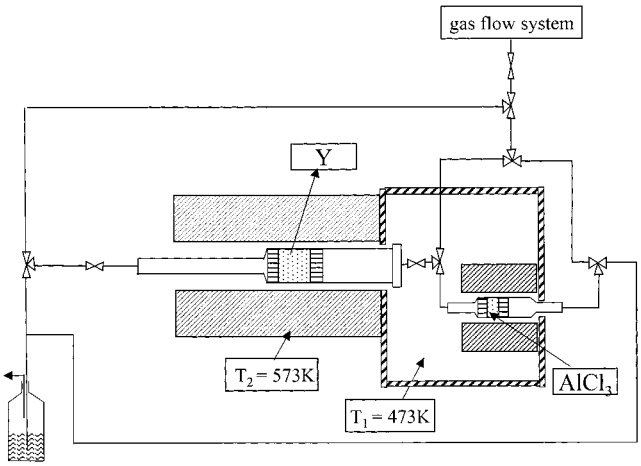


**Figure 1.** Experimental setup for alumination and dealumination of zeolite material.

For the FAU samples, a detailed characterization has been published by Remy et al.[9] They are commercially available and general data are known about their preparation procedure: CBV712 (Si/Al = 6) is obtained by mild acid leaching of the steamed $NH_4$−Y zeolite; CBV720 (Si/Al = 15) and CBV780 (Si/Al = 40) are steamed a second time and leached with a mineral acid.

For the aluminated, dealuminated and exchanged samples, the starting material was a siliceous zeolite Y with a Si/Al ratio of 3.6. This sample was a gift from Exxon Chemical Europe. $NH_4^+$-exchange of the $Na^+$-zeolites was performed in $NH_4Cl$ (*pro analyse*, Merck) solutions with a 10-fold excess of $NH_4^+$ with respect to the cation exchange capacity (CEC) at a solid: liquid ratio of 1 g/dm$^3$. The samples were exchanged 3-times overnight under continuous stirring and washed with bidistilled water until $Cl^-$-free. The residual sodium content of the zeolite was determined by chemical analysis and corresponds to Na/Al < 0.20. $Al^{3+}$-exchanged and $La^{3+}$-exchanged zeolite Y were prepared in the same manner using aqueous $AlCl_3 \cdot 6H_2O$ (*pro analyse*, UCB) and $La(NO_3)_3 \cdot 6H_2O$ (*pro analyse*, Janssen Chimica) solutions.

**2. Aluminated Zeolites.** The alumination procedure was similar to that reported by Chang et al.[30] The setup used for alumination is presented in Figure 1. Several three-way stopcocks allow the carrier gas to flow in both directions through the reaction tube. The furnace, which is a bit shorter than the reaction tube, could be moved to either end of the reaction tube. In this way, the unheated section constitutes of an air condenser, which serves as a collector of the unreacted aluminum chloride. In a standard experiment, 1.5 g of zeolite was loaded in the horizontal quartz tube and calcined at 773 K for 10 h in an oxygen flow of 50 mL/min. At the reaction temperature (573 K) the helium flow was diverted through a bed of anhydrous $AlCl_3$ powder (*pro analyse*, Johnson Matthey) placed in a second quartz tube and kept at 473 K using a homemade heating box. The helium carrier gas containing $AlCl_3$ vapor passed through the zeolite bed at the reaction temperature and induced alumination. After 2 h, the furnace was moved to the other end of the tube and the flow was reversed for another 2 h. Finally, the temperature was raised to 673 K and the sample was purged with helium for 1 h to remove all the unreacted $AlCl_3$ from the zeolite. After cooling to room temperature in a helium flow, the sample (AlY) was transferred into an EPR quartz cell, in a nitrogen glovebox.

**3. Steamed Zeolites.** The steamed samples were prepared using the same setup as described above, but the $AlCl_3$ tube was replaced by a water-bubbler. Two samples were prepared: (1) a severely steamed zeolite Y (SY1) prepared at 923 K with a contact time of 6 h and $H_2O$ partial pressure of 700 Torr and (2) a mildly steamed zeolite Y (SY2) prepared at 773 K with a contact time of 20 h and $H_2O$ partial pressure of 100 Torr.

**4. Techniques.** In situ FTIR spectra were recorded in the region 4000−1000 cm$^{-1}$ on a Nicolet 730 spectrometer, equipped with a DTGS detector, using a homemade cell and thin self-supported wafers (8−10 mg/cm$^2$). One-hundred scans were accumulated for acquiring one spectrum with a resolution of 1 cm$^{-1}$. The cell was connected to an evacuation-gas flow system, which allowed treatments up to 500 °C, when the $CaF_2$ windows were cooled with circulating tap water. Low-temperature measurements (113 K) were performed by placing the wafer in a special holder that is cooled with liquid nitrogen. The samples were first calcined overnight in $O_2$ and then evacuated ($7.5 \times 10^{-6}$ Torr) for 1 h at 773 K. FTIR spectra of the samples were recorded before and after adsorption of 30 Torr of CO (99.99%, Air Liquide), as well as in a dynamic regime, with increasing evacuation time at low temperature.

X-ray powder diffractograms were obtained using a Siemens D5000 X-ray diffractometer with Cu Kα radiation. The $^{27}$Al magic angle spinning nuclear magnetic resonance (MAS NMR) measurements were performed on a Bruker MSL-400 spectrometer with a magnetic field strength of 9.4 T and a resonance frequency of 104.26 MHz. The spectra were recorded with 0.1 s delay time, a pulse length of 0.6 $\mu$s and a magic angle spinning frequency of 12 kHz. A 0.5 M $Al(NO_3)_3$ (*pro analyse*, Fluka) solution was used as a reference.

EPR spectra were recorded at 115 K on a Bruker ESP300E spectrometer in X-band (9.5 GHz) with a double rectangular $TE_{104}$ mode cavity. The modulation frequency and amplitude were 100 kHz and 5 G, respectively. The EPR spectra were double integrated using Bruker software and the spin concentrations were determined relative to a reference standard. This standard sample is USY CBV720 loaded with different $V^{4+}$ amounts, using the wet impregnation method with a vanadyl sulfate salt ($VOSO_4 \cdot H_2O$, 96%, Janssen Chimica). The absolute accuracy of the EPR quantification is better than 30%, while the relative accuracy of the spin concentrations between the different samples under investigation must be about 5%.[31]

The standard pretreatment procedure involved sample calcination in an $O_2$ flow at 773 K for 10 h and sample degassing ($7.5 \times 10^{-6}$ Torr) at 773 K for 2 h. For one set of experiments the degassing temperature was varied between 673K and 973K. 1.2 Torr of NO (≥ 99%, Air Liquide) at 293 K was admitted

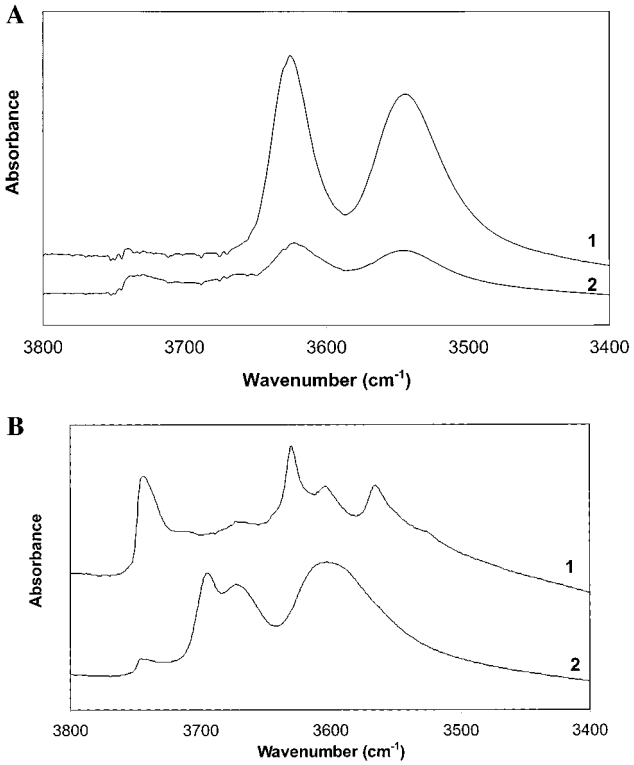


**Figure 2.** (A) FTIR spectra of the hydroxyl region of the samples Y (1) and AlY (2). (B) FTIR spectra of the hydroxyl region of the samples SY2 (1) and CBV712 (2).

into the EPR cell (volume of 26 mL) over a 0.2 g sample. To adsorb uniformly the NO, the sample was cooled by slowly immersing the tube in liquid nitrogen, prior to recording the EPR spectrum.

The EPR spectra were simulated with a program developed at the Illinois EPR Center based on matrix diagonalization, which generates a powder spectrum taking into account the hyperfine (HFS) and the super-hyperfine interaction (SHFS).[32] The fitting routine uses the simplex method to minimize the standard deviation between the experimental and the calculated EPR spectrum.

## Results

**1. Framework and Nonframework Aluminum in Zeolites.** Table 1 gives an overview of the total Al content and the amount of framework and nonframework Al as determined by chemical analysis and $^{27}$Al MAS NMR measurements. The amount of nonframework aluminum was calculated as the difference between the total amount of aluminum and the amount of framework Al. As expected, the highly crystalline zeolite Y does not contain any nonframework Al. Alumination of this sample leads to an increase of the amount of nonframework Al to about 0.26 mmol Al/g. The highest amount of nonframework Al is obtained by severe dealumination. Also the commercially, partially leached USY sample (CBV 712) contains a lot of nonframework Al.

The infrared spectra in the O−H stretching region of the parent sample (Y) and the aluminated one (AlY) are presented in Figure 2A. In the spectrum of the AlY the bands assigned to OH-groups (3640 and 3560 cm$^{-1}$) are less intense, which is an indication that the $Al^{3+}$-ions are partially replacing the protons (Scheme 1). The band assigned to the silanol groups (3745 cm$^{-1}$) remains very small, which means that no defect sites are created in the lattice during such treatments. This is in line with

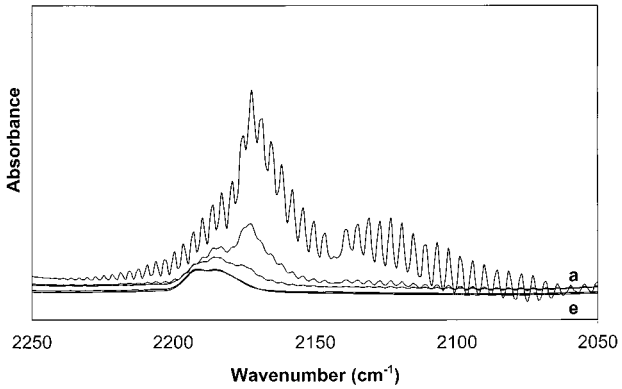


**Figure 3.** FTIR spectra of CO adsorbed at 113 K on CBV3020. (a) Equilibrium pressure of 30 Torr and under dynamic vacuum with increasing evacuation time ((b) 5 min, (c) 10 min, (d) 45 min, and (e) 1 h).

**SCHEME 1**

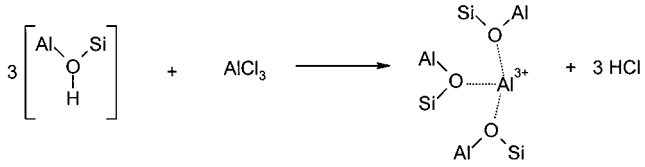


the results of the XRD measurements that indicate a well-preserved crystallinity after alumination. The FTIR spectra of the steamed zeolite SY2 and ultrastable zeolite CBV712 are presented in Figure 2B. These spectra are typical for samples containing extraframework Al. As can be found in the literature,[33] bands can be assigned to silanol groups (3750 cm$^{-1}$), bridging hydroxyls (3630 and 3570 cm$^{-1}$) and OH groups associated with extraframework aluminum species (around 3700, 3670, and 3525 cm$^{-1}$). For all samples, the XRD diffractograms show high crystallinity.

**2. Probing Lewis Acidity with CO at Low Temperatures.** FTIR spectra in the CO stretching region are presented as the difference between the spectra of the zeolites with adsorbed gas and those of the calcined wafers prior to CO adsorption, measured at low temperatures. The spectra of the adsorbed CO gas were measured in a dynamic regime, under evacuation.

Figure 3 presents the FTIR spectra of the CO adsorbed species (30 Torr, 113K) on CBV3020, for increasing evacuation time. Because of the interaction of the CO molecule with the adsorption sites, its stretching frequency is shifted to higher wavenumbers with respect to the gas-phase value of 2143 cm$^{-1}$. This gas-phase spectrum shows a rotovibrational band centered around 2143 cm$^{-1}$. The stronger the interaction with the adsorption site, the larger the frequency shift. The intense band at around 2172 cm$^{-1}$, which is disappearing after a relatively short evacuation time is due to weakly bounded CO molecules, such as CO interacting with Brönsted acid sites.[1,4] This assignment is confirmed by the IR spectra in the O−H stretching region of zeolite Y with the increasing evacuation time (Figure 4). The formation of the O−H···CO complex causes a shift of about 300 cm$^{-1}$ in the hydroxyl stretching frequency toward lower wavenumbers. This is observed only for the acidic OH groups in the supercages and not for those in the sodalite cages, which are not accessible for CO molecules at low temperatures.[5] The less acidic OH groups bound to the nonframework Al species are not perturbed either. Figure 4 shows that the initial OH band is restored with increasing evacuation time. There is a simultaneous disappearance of the 2172 cm$^{-1}$ band in the CO

**TABLE 2: The Assignments of CO Bands in the LAS Frequency Domain (2175−2208 cm$^{-1}$) and Their Relative Intensities Normalized to the Total Area of the LAS Region in the Spectrum**

| | assignments of CO bands (cm$^{-1}$) in the LAS region and their relative intensities (%) | | | | |
|---|---|---|---|---|---|
| sample | C 2175−2176 | $L_1$ 2179−2180 | $L_2$ 2183-2186 | $L_3$ 2190−2192 | $L_4$ 2197−2208 |
| Y | 94.4 | 5.6 | | | |
| CBV712 | 6.2 | 49.3 | 44.5 | | |
| CBV720 | 0.9 | 40.5 | 27.0 | 30.9 | 0.7 |
| CBV780 | 0.6 | 43.0 | 15.5 | 40.4 | 0.4 |
| SY1 | 77.6 | 15.7 | | 6.7 | |
| SY2 | 0.5 | 27.7 | 41.6 | 21.0 | 9.2 |
| AlY | 45.7 | 19.9 | 13.9 | 8.0 | 12.5 |
| $Al_{ex}Y$ | 58.0 | 15.7 | | 2.2 | 24.1 |
| LaY | 98.0 | | 1.5 | 0.5 | - |
| CBV3020 | | 23.7 | 29.6 | 39.5 | 7.2 |
| CBV5020 | | 25.5 | 25.9 | 38.7 | 9.9 |
| CBV8020 | 0.4 | 32.5 | 43.2 | 23.9 | - |

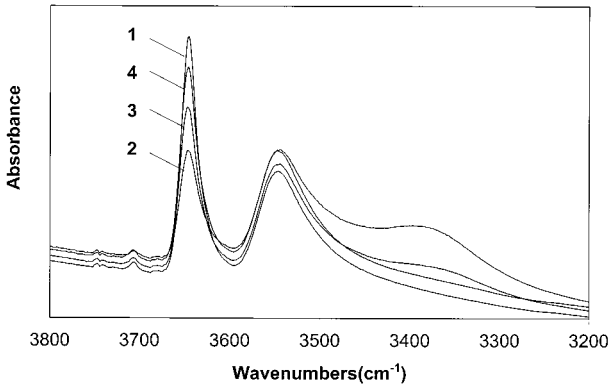


**Figure 4.** FTIR spectra of the hydroxyl region: (1) Y calcined and evacuated ($7.5 \times 10^{-6}$ Torr) at 773 K; (2) CO (30 Torr) at 113 K on Y; (3) dynamic vacuum, 5 min; and (4) dynamic vacuum, 2 h.

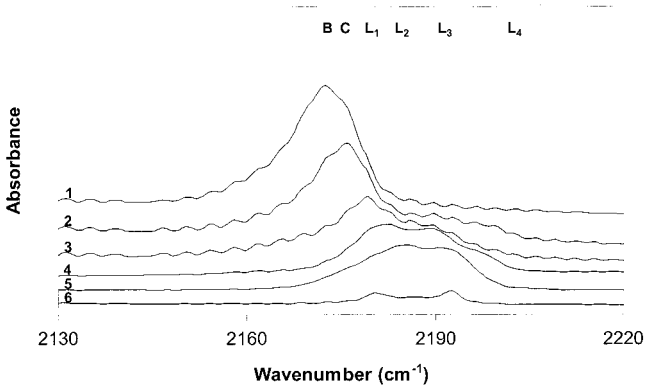


**Figure 5.** FTIR spectra of CO adsorbed at 113 K on FAU and MFI zeolites, under dynamic vacuum ($7.5 \times 10^{-6}$ Torr), 45 min: (1) Y, (2) AlY, (3) CBV712, (4) SY2, (5) CBV3020, and (6) CBV780.

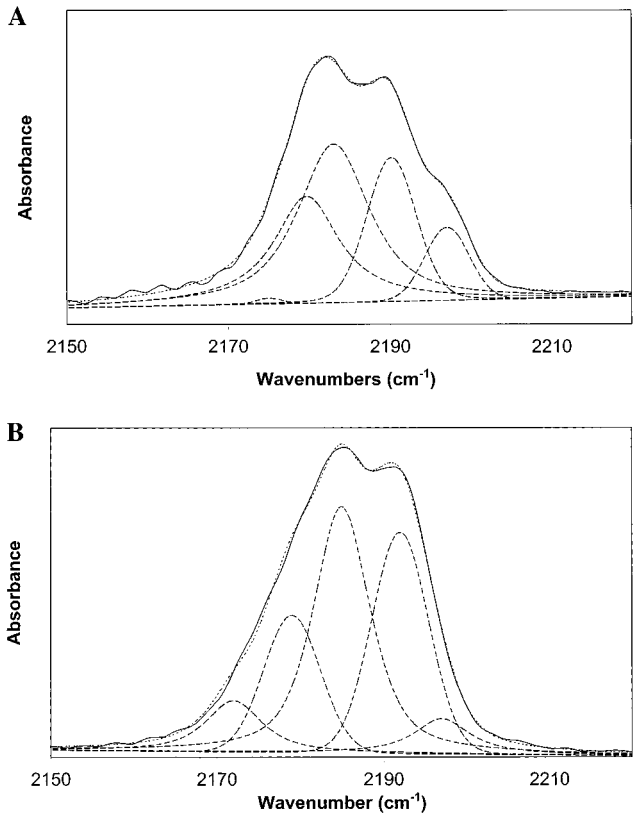


**Figure 6.** The experimental and the fitted FTIR spectra of CO adsorbed on (A) SY2 and (B) CBV3020. The individual absorption lines are also shown.

spectra. This correlation confirms the assignment given to the 2172 cm$^{-1}$ band.

In Figure 3 we have assigned the bands between 2175 and 2208 cm$^{-1}$ to CO adsorbed at Lewis acid sites.[1] This spectral region will be further referred as the LAS region. With increasing evacuation time, only two bands can be clearly distinguished, indicating the existence of at least two Lewis acid sites with different strengths.

Upon evacuation the band maximum of the CO stretching frequency shifts to higher wavenumbers and the overall intensity decreases. Six frequency regions can be identified in this way. They are denoted as B, C, and $L_1-L_4$ in Figure 5. Band B at 2172 cm$^{-1}$ is CO H-bonded with bridging hydroxyls in the supercages (see above), Band C at 2175−2176 cm$^{-1}$ has been ascribed to CO interacting with residual exchangeable cations.[1,4,5] The $L_1-L_4$ regions are due to CO adsorbed on Lewis acid sites. The increase of the frequency of the CO stretch is an indication of the increase of the strength of interaction. $L_1$, $L_2$, and $L_3$ are clearly discernible as peaks in the regions 2179−2180, 2183-2186, and 2190−2192 cm$^{-1}$, respectively. $L_4$ in the region 2197−2208 cm$^{-1}$ is not clearly visible, and it is uncertain whether a physical interpretation must be sought. Between the zeolite samples under investigation only the relative intensities of the peaks in these six regions are different, and Table 2 lists the relative intensities (%) of the bands with respect to the total integrated intensity of each spectrum in the LAS region (2175−2208 cm$^{-1}$). These calculations as well as the curve fitting were performed with the *Spectracalc/386* program (Galactic Industries, Inc.) using Gaussian−Lorentzian line shapes. Two illustrative examples of deconvoluted spectra, corresponding to CO adsorbed on SY2 and CBV3020 are presented in Figure 6.

The data shown in Table 2 indicate that the relative intensities of the bands assigned to CO adsorbed on the stronger Lewis

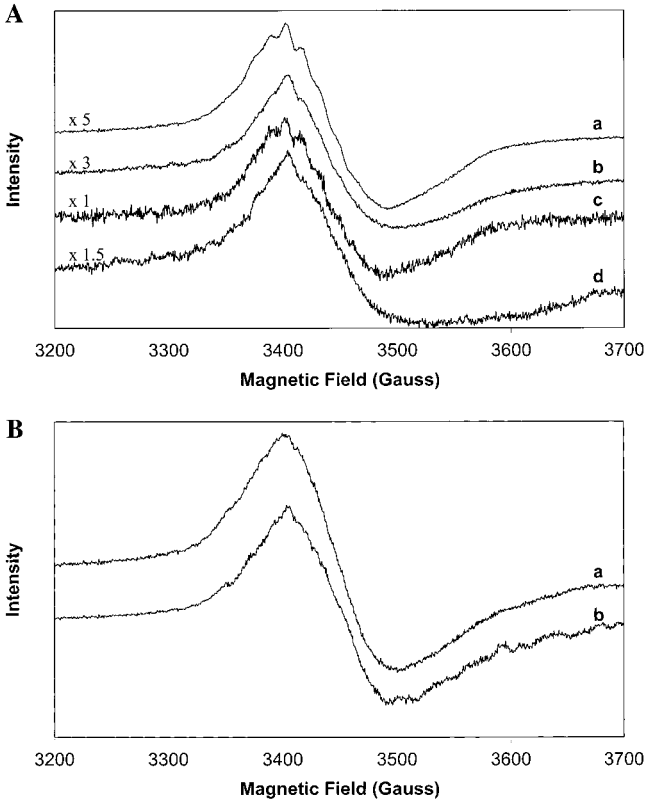


**Figure 7.** (A) EPR spectra of NO (1.2 Torr, 115K) adsorbed on (a) CBV720, (b) CBV712, (c) CBV780, and (d) LaY. (B) EPR spectra of NO (1.2 Torr, 115 K) adsorbed on (a) CBV3020 and (b) CBV5020.

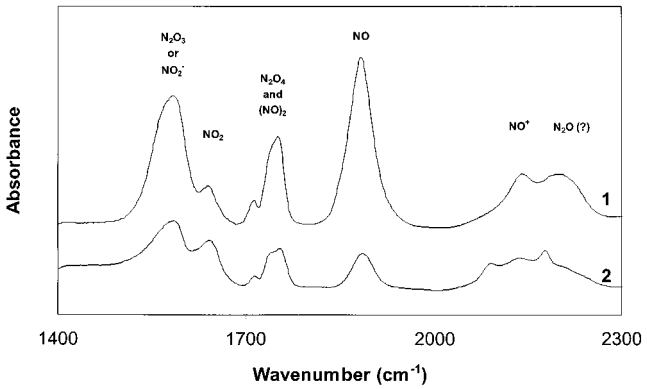


**Figure 8.** FTIR spectra of adsorbed NO (30 Torr) at 113 K: (1) CBV3020 and (2) CBV712.

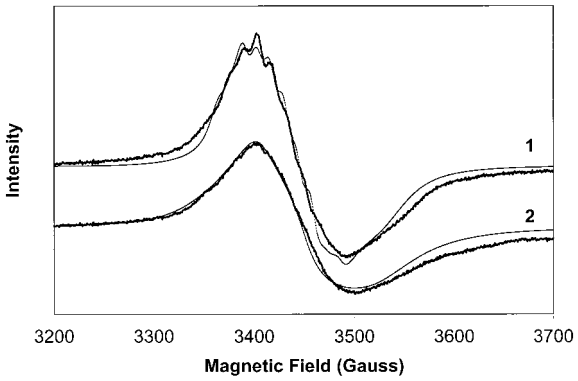


**Figure 9.** Experimental (full line) and simulated (dotted line) EPR spectra of adsorbed NO on CBV720 (1) and CBV3020 (2).

sites increase with increasing amount of nonframework aluminum. This is the case for AlY and SY2. The presence of relatively strong Lewis sites both in the aluminated and the dealuminated samples is expected, since nonclustered and uniformly distributed nonframework Al species are created in these samples. In the case of the mildly steamed zeolite Y, stronger sites are created and they are more accessible to adsorbed CO than those present in the severely steamed sample or in the CBV-series before leaching (CBV712). It is worthy to mention that all these statements referring to the site strength are based only on spectroscopic data; i.e., frequency shifts.

**3. Probing Lewis Acidity with NO at Low Temperatures.** The EPR spectra shown in Figure 7 are typical for NO adsorbed on Lewis acid sites and are characterized by a hyperfine interaction due to the nitrogen nucleus ($^{14}$N, $I = 1$) and a superhyperfine interaction due to the neighboring aluminum atoms ($^{27}$Al, $I = {}^5/_2$). The lines are broad and the interactions are not always resolved and in any case weak. The EPR spectra are recorded after NO adsorption (1.2 Torr) at 115 K on FAU (A) and MFI (B) zeolites. Before NO adsorption all samples were pretreated as specified in the Experimental Section. The spectra are typical for an Al−NO adsorbate complex with a rhombic symmetry.

Only a part of the supplied NO is EPR-active and different EPR-silent species are generated, which can be observed in the corresponding FTIR spectra (Figure 8). The assignments to specific nitrogen oxide species, based on a recent review paper of Hadjiivanov,[34] are given in Figure 8. It shows the formation of $N_2O_3$ or $NO_2$-, $NO_2$, $N_2O_4$, $(NO)_2$, NO, and $NO^+$.

The EPR spectra were simulated[32] in order to calculate the *g*-factors and the hyperfine splitting constants of Al ($^{Al}$A) and N ($^{N}$A). The starting values were estimated from the experimental spectra and then, via an iterative procedure, optimized until a good fit of the experimental data was obtained. Figure 9 presents the experimental and the simulated spectra of the CBV720 and CBV3020 samples. The obtained EPR parameters are summarized in Table 3. One can notice that the *g*-values are dependent on the structure type and on the aluminum content of the zeolite. For the FAU structure values of 1.999 and 1.997 are typical for $g_{xx}$ and $g_{yy}$, respectively, while the $g_{zz}$ value varies from 1.932 for CBV712 to 1.940 for CBV780. The type of the nonframework aluminum species is also important: the $g_{zz}$ value varies from 1.922 for severely steamed sample to 1.932 for the mildly steamed zeolite Y. The exchanged zeolites have lower $g_{zz}$ values than the aluminated one: 1.928 and 1.905 for $Al_{ex}Y$ and, respectively, LaY. For the MFI samples the typical *g*-values are $g_{xx} = 1.995$, $g_{yy} = 1.994$, and $g_{zz} = 1.940$. The variation of the signal shape with Lewis acid strength is less visible, but there are significant differences in the EPR signal intensity, namely, the EPR signal is more intense for the lowest Si/Al ratio.

The EPR spectra were doubly integrated and the resulting intensities (Table 3) were correlated for each structure type with the amount of the nonframework aluminum species determined from $^{27}$Al MAS NMR measurements and chemical analysis (Table 1). Figure 10 presents the dependence of the doubly integrated intensities (D. I. I.) on the amount of nonframework aluminum for FAU and MFI samples. Taking into account that the relative accuracy of the spin concentration determinations is about 5%, a clear maximum is observed at 0.15 mmol Al/g for the CBV720 sample. Thus, the number of LAS−strong enough to quench the orbital magnetic moment of NO− gradually increases with an increasing amount of nonframework Al in the zeolite material. There is no relation between higher amounts of nonframework Al in the zeolite material and the

**TABLE 3: Parameters of the Simulated EPR Spectra and Spin Concentrations**

| sample | $g_{xx}$ | $g_{yy}$ | $g_{zz}$ | $\Delta g_{zz} = g_e - g_{zz}$ | $^{N}A_{xx,yy}$ (G) | $^{Al}A_{xx,yy}$ (G) | $c_s$ ($\times 10^{18}$ spins/g) |
|---|---|---|---|---|---|---|---|
| Y | 1.996 | 1.996 | 1.928 | 0.074 | 26.7 | 8.5; 19.2 | 0.19 |
| CBV712 | 1.999 | 1.997 | 1.932 | 0.070 | 30.9 | 6.5; 21.5 | 1.03 |
| CBV720 | 1.999 | 1.997 | 1.939 | 0.064 | 27.1 | 13.6; 13.6 | 1.67 |
| CBV780 | 1.999 | 1.997 | 1.940 | 0.062 | 29.2 | 12.6; 12.6 | 0.52 |
| SY1 | 1.999 | 1.997 | 1.922 | 0.080 | 30.9 | 6.5; 21.5 | 0.60 |
| SY2 | 1.999 | 1.997 | 1.932 | 0.070 | 30.9 | 6.5; 21.5 | 0.77 |
| AlY | 1.999 | 1.997 | 1.935 | 0.067 | 30.9 | 6.5; 21.5 | 0.75 |
| $Al_{ex}Y$ | 1.999 | 1.997 | 1.928 | 0.074 | 30.7 | 9.4; 9.4 | 0.85 |
| LaY | 1.999 | 1.990 | 1.905 | 0.097 | 35.9 | 7.9; 7.9 | 0.91 |
| CBV3020 | 1.995 | 1.994 | 1.940 | 0.062 | 30.7 | 9.0; 21.5 | 1.03 |
| CBV5020 | 1.995 | 1.994 | 1.940 | 0.062 | 35.7 | 8.7; 21.5 | 0.96 |
| CBV8020 | 1.995 | 1.994 | 1.940 | 0.062 | 35.7 | 8.7; 21.5 | 0.54 |

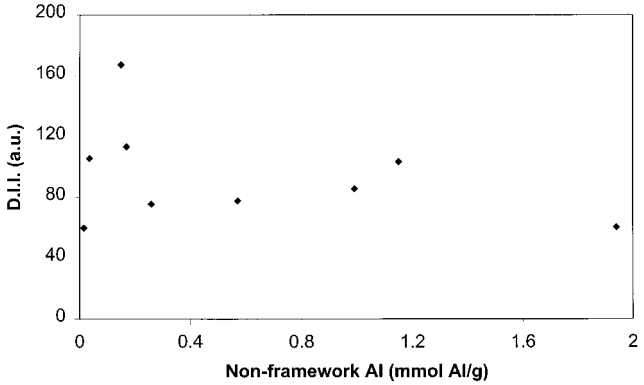


**Figure 10.** Double integrated intensities of the EPR signal of adsorbed NO (measured at 115 K) as a function of the nonframework Al content of the samples.

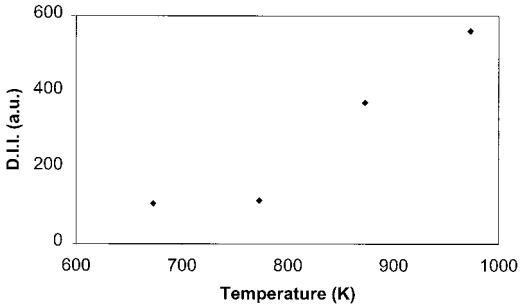


**Figure 11.** Double integrated intensities of the EPR signal of adsorbed NO (measured at 115 K) as a function of the pretreatment temperature of CBV 712 sample.

amount of LAS as detected by the ESR technique. This observation can be explained by the formation of clustered Al species, which diminish the number of LAS and hinder their accessibility for probe molecules, such as NO.

For the CBV720 sample the pretreatment temperature was increased above 800 K in steps of 100 K. As a consequence, the doubly integrated intensities of the EPR signal increased significantly, although the shape of the signal was not essentially changed. The dependence of the doubly integrated intensity of the EPR signal on the pretreatment temperature indicates a steady increase with pretreatment temperature (Figure 11).

## Discussion

**1. Alumination of Zeolite Y.** The reaction of gaseous $AlCl_3$ with zeolites was previously used for aluminum insertion in the framework, via the defect sites, in the case of zeolite Y, ZSM-5, and mordenite.[30,35−38] Using a parent material without defect sites and mild reaction conditions (low temperature, low partial pressure of gaseous $AlCl_3$), we succeeded to insert aluminum in nonframework positions. The aluminum chloride interacts with the protons of the bridging OH groups, leading to the formation of nonframework aluminum species and HCl, which was removed with the flow of carrier gas (Scheme 1). Keeping the reaction temperature below 573K and using a continuous flow of dry helium to eliminate the unreacted aluminum chloride were crucial for inserting aluminum without altering the crystallinity of the zeolite.

**2. Probing Lewis Acidity with CO at Low Temperatures.** When adsorbed, the interaction between the CO dipole and the electric field at the adsorption site strengthens the C−O bond and causes the increase in the C−O stretching frequency above that of the free molecule.[13,19] Theoretical calculations have shown that the interaction via the carbon atom is stronger, independently of the acid site model used.[16,21] Moreover, a Lewis site produces a stronger complex than a Brönsted site, which in turn produces stronger complexes than the silanol group.[21] Our findings for all the samples investigated in this work support the above statements.

Huber and Knözinger[5] have shown that the oxygens surrounding the electron acceptor site and the coordination symmetry of adsorbed CO influence the polarization and, consequently, the shift of the CO stretching vibration. Therefore, we assume that the zeolite structure, and the distribution of the $SiO_4$ and $AlO_4$ tetrahedra play an important role in the definition of Lewis acid sites. Moreover, the aluminum content (Si/Al ratio) will influence the intensity of the electric field in the vicinity of the acceptor sites, which is consequently reflected in the observed frequency shift.

From the infrared results one may conclude that within the same structure type, the Si/Al ratio and the amount of nonframework aluminum are the factors determining a particular infrared spectrum; i.e., the higher the amount of nonframework aluminum, the more intense are the adsorbed CO peaks in the LAS region, as in the case of CBV712, SY2, and CBV3020. When part of the nonframework aluminum is leached, as in the case of CBV720 and CBV780, the strong sites are still present ($L_3$ and $L_4$), but the spectra are less intense. The highest shift in frequency ($L_4$) is observed in the case of aluminated and mildly steamed zeolite Y, as well as in the exchanged $Al_{ex}Y$. This can be possibly explained by the presence of Al species with highly distorted symmetry and by the accessibility of the nonframework Al species resulting from these methods. The samples belonging to the commercial CBV series have only small amounts of the strongest site, in the partially leached samples. The severely steamed zeolite Y has less strong Lewis acid sites, probably due to the clustering of the nonframework Al species, resulting in bulky entities that block the access of the CO molecules inside the zeolite cavities.

The NMR results show also that via severe steaming an important percentage (53%) of the initially tetrahedrally coor-

dinated aluminum is transformed into octahedrally and distorted octahedrally coordinated aluminum. This happens to a much smaller extent (19%) in the case of the mildly steamed zeolite Y.

CO molecules adsorbed on the MFI samples present CO stretching bands in the same frequency range as those of the Y zeolites and their intensities are also dependent on the Si/Al ratio. The lower the Si/Al ratio, the higher is the total aluminum content and thus, the higher is the amount of aluminum found as nonframework species. The latter species act as Lewis sites of different strengths ($L_1-L_4$).

All the peaks corresponding to CO adsorbed on LAS are less intense than those assigned to CO adsorbed on BAS. However, these apparently weak absorptions do not necessarily mean small concentrations. One cannot make any assumption about the Lewis acid site concentrations, unless the extinction coefficients are first taken into account. In the adsorbed state, the electronic distribution in CO is perturbed toward that characteristic of a homopolar molecule. The stronger the site the more significant is the perturbation that reduces the dynamic dipole moment of the adsorbed CO species. Consequently, the extinction coefficient, which is proportional with the square of the dynamic dipole moment, is also decreased. On the basis of the above considerations and on comparative studies between adsorption of $N_2$ and CO, Wakabayashi et al.[19] proposed for the extinction coefficient of CO on LAS a value equal to $^1/_3$ of that corresponding to CO on BAS.

The CO species adsorbed on LAS at frequencies higher than 2175 $cm^{-1}$ have small extinction coefficients. Therefore, one can hardly make assumptions about the absolute concentration of the Lewis acid sites, based only on the infrared study of adsorbed CO. However, the method remains important for its sensitivity in distinguishing Lewis acid sites with different strengths and as a tool for estimating the relative concentrations of the different LAS within a series of structurally related samples.

**3. Probing Lewis Acidity with NO at Low Temperatures.** The electric field associated with the Lewis acid site removes the degeneracy of the $\pi$ orbitals of the adsorbed NO molecule, and the molecule becomes EPR active. According to theoretical calculations,[22] the value of $g_{zz}$ (assuming that the magnetic field is parallel to the N−O axis) is a measure of the splitting induced by the crystal field. In this way, the strength of the probed acid site can be correlated with the $g_{zz}$ value of the recorded spectrum. The stronger the electric field of the Lewis acid site, the smaller the difference $\Delta g_{zz} = g_e - g_{zz}$, where $g_e$ is the free electron value (2.0023).

Generally, the EPR spectrum of NO adsorbed on a LAS is characterized by hyperfine interaction due to the nitrogen nucleus and superhyperfine interactions due to the neighboring aluminum nucleus. The latter interaction splits each of the nitrogen hyperfine lines into six lines, thus the polycrystalline spectrum should be rather complex. In reality, the lines are broad and the hyperfine structure is only partially resolved at 115 K.

Despite the broad spectra, reasonably accurate values for the g and A tensors are obtained by simulation. We have followed the model proposed by Kasai and Bishop,[23] modified by Gutsze et al.[26] The NO molecule bound to a LAS, is able to rotate around the $z$ axis (N−O direction) or around the $Al^{3+}-N$ direction. Consequently, the components of the **g**-tensor are $g_{xx} \cong g_{yy} > g_{zz}$ and those of the hyperfine tensor are $^{N}A_{xx} \cong {}^{N}A_{yy}$, $^{N}A_{zz} \cong 0$. For the superhyperfine structure we found, in most of the cases, different values for $^{Al}A_{xx}$ and $^{Al}A_{yy}$, and $^{Al}A_{zz} \cong 0$. The absorption lines were Gaussian with a line width of 15−120 G.

For the USY series, the strength of the Lewis acid sites is increasing with the successive leaching procedures. As can be seen in Table 3, CBV780 has stronger sites than CBV712. Also, one may notice that the Al hyperfine structure is more visible for the samples having more isolated sites, namely, CBV720 and CBV780. Further, the aluminated zeolite Y has stronger sites than the mildly steamed zeolite Y, which in turn has stronger sites than the severely steamed one. Both dealuminated zeolites Y have stronger sites than the cation exchanged ones, irrespective of the cation type. As in the case of the adsorbed CO, the intensity of the signal is increasing with the amount of nonframework aluminum up to a certain value, when the nonframework aluminum species start to hinder the access of the probe molecules. At the same time, with increasing Si/Al ratio the Lewis acid sites are stronger. The remarkably strong sites of the aluminated zeolite Y are evidenced also by this method.

The $g_{zz}$ values listed in Table 3 indicate that MFI zeolites have strong sites, comparable with those of highly dealuminated zeolite Y. Within the CBV series the intensity of the signal is increasing with the amount of nonframework aluminum.

However, the estimated spin concentrations relative to the standard samples are much lower than expected (Table 3). If we try to estimate the upper limit of the Lewis sites concentration, assuming that each nonframework aluminum atom is a potential Lewis site, then the EPR results are probing 0.2−6.0% of the total number of sites, depending on the investigated sample. This is of course a rough estimation, since not every nonframework aluminum atom is a Lewis site. One may have pairs, or clusters of aluminum atoms, or different other combinations including oxygen and/or hydroxyl groups. Moreover, not all the sites are accessible, especially in the samples with high nonframework aluminum content.

There are several reasons that can explain the severe underestimation of the Lewis acid sites concentration: (1) the competition between NO and the $N_xO_y$ species formed as a result of chemical interaction at the adsorption site; (2) the different sorption geometries and sorption strengths are not always favorable to the quenching of the orbital motion of the NO molecule; (3) high NO pressure favors the formation of diamagnetic $N_2O_2$ dimers on the adsorption sites.

The number of Lewis acid sites detected with the EPR technique is increasing with the pretreatment temperature. The progressive dehydroxylation, with the formation of an increased number of sites with a distorted electrical field, which act as electron accepting sites is at the origin of this process. Although an important increase in intensity can be observed, there was no change in the shape of the signal. This is an indication that the generated sites are not stronger than existing ones.

## Conclusions

FTIR and EPR of adsorbed probe molecules were used to study Lewis acid sites in FAU and MFI zeolites with different nonframework Al content.

Infrared spectra of adsorbed CO at low temperatures give information about all types of sites present on the samples. The absorption bands were assigned to CO fixed on Brönsted sites, cations and true Lewis acid sites with different strengths. The frequency shifts and the relative intensities of the peaks were related with the structure type and the nonframework aluminum content of the investigated samples. The peak intensities of adsorbed CO on Lewis acid sites are weak, because of the small

extinction coefficients in that frequency range. CO adsorption at low temperature has a good sensitivity in identifying LAS with different strengths. When studying structurally related samples, the method can be used for estimating the relative concentrations of the different LAS.

In contrast, EPR of adsorbed NO is probing only the sites strong enough to quench the orbital magnetic moment of NO. The method can provide an estimation of the strength of the detected Lewis acid sites, via the $g_{zz}$ parameter. A correlation was established between the amount of nonframework Al and the spin concentrations of adsorbed NO. These concentrations are lower than the expected number of Lewis acid sites.

Several methods were proposed for creating Lewis acid sites in a controlled way. Alumination with $AlCl_3$ leads to well-distributed nonframework Al species with a highly distorted geometry, which act as strong Lewis acid sites. The mild steaming procedure leads to similar sites and a high concentration of nonframework Al. Although high, the amount of Al extracted from the framework with the severe steaming procedure is less effective in creating strong LAS, most probably because the clustered Al species block the access of the probe molecules to the active sites.

**Acknowledgment.** B. M. W. is a fellow of the Fonds voor Wetenschappelijk Onderzoek-Vlaanderen (F. W. O.). The authors thank Dr. B. Wouters and Prof. P. Grobet for the $^{27}Al$ MAS NMR measurements and H. Leeman for technical assistance.

## References and Notes

(1) Zecchina, A.; Otero Arean, C. *Chem. Soc. Rev.* **1996**, 187. Brunner, E. *Catal. Today* **1997**, *38*, 361. Zecchina, A.; Lamberti, C.; Bordiga, S. *Catal. Today* **1998**, *41*, 169. Giamello, E. *Catal. Today* **1998**, *41*, 239. Busca, G. *Catal. Today* **1998**, *41*, 191. Coluccia, S.; Marchese, L.; Martra, G. *Microporous Mesoporous Mater.* **1999**, *30*, 43. Busca, G. *Phys. Chem. Chem. Phys.* **1999**, *1*, 723.

(2) Bordiga, S.; Platero, E. E.; Arean, C. O.; Lamberti, C.; Zecchina, A. *J. Catal.* **1992**, *137*, 179.

(3) Kuroda, Y.; Maeda, H.; Yoshikawa, Y.; Kumashiro, R.; Nagao, M. *J. Phys. Chem.* **1997**, *101*, 1312.

(4) Hadjiivanov, K.; Knözinger, H. *Chem. Phys. Lett.* **1999**, *303*, 513.

(5) Huber, S.; Knözinger, H. *Appl. Catal. A: General* **1999**, *181*, 239.

(6) Bordiga, S.; Turnes Palomino, G.; Paze, C.; Zecchina, A. *Microporous Mesoporous Mater.* **2000**, *34*, 67.

(7) Jacobs, P. A.; Beyer, H. K. *J. Phys. Chem.* **1979**, *83*, 1174.

(8) Pöppl, A.; Rudolf, T.; Michel, D. *J. Am. Chem. Soc.* **1998**, *120*, 4879.

(9) Remy, M. J.; Stanica, D.; Poncelet, G.; Feijen E. J. P.; Grobet, P. J.; Martens, J. A.; Jacobs, P. A. *J. Phys. Chem.* **1996**, *100*, 12440.

(10) Shannon, R. D.; Gardner, K. H.; Staley, R. H.; Bergeret, G.; Gallezot, P.; Auroux, A. *J. Phys. Chem.* **1985**, *89*, 4778.

(11) Pelmenschikov, A. G.; van Santen, R. A.; Jänchen, J.; Meijer, E. *J. Phys. Chem.* **1993**, *97*, 11071.

(12) Morterra, C.; Bolis, V.; Magnacca, G. *Langmuir* **1994**, *10*, 1812.

(13) Ballinger, T. H.; Yates, J. T. Jr. *Langmuir* **1991**, *7*, 3041.

(14) Ishida, S.; Inamura, S.; Fujimura, Y. *React. Kinet. Catal. Lett.* **1991**, *43*, 447.

(15) Concepcion, P.; Reddy, B. M.; Knözinger, H. *Phys. Chem. Chem. Phys.* **1999**, *1*, 3031.

(16) Gruver, V.; Fripiat, J. J. *J. Phys. Chem.* **1994**, *98*, 8549. Gruver, V.; Panov, A.; Fripiat, J. J. *Langmuir* **1996**, *12*, 2505.

(17) Morterra, C.; Cerrato, G.; Bolis, V.; Di Ciero, S.; Signoretto, M. *J. Chem. Soc., Faraday Trans.* **1997**, *93*, 1179.

(18) Bordiga, S.; Garrone, E.; Lamberti, C.; Zecchina, A.; Arean, C. O.; Kazansky, V. B.; Kustov, L. M. *J. Chem. Soc., Faraday Trans.* **1994**, *90*, 3367.

(19) Wakabayashi, F.; Kondo, J. N.; Domen, K.; Hirosi, C. *J. Phys. Chem.* **1995**, *99*, 10573.

(20) Kustov, L. M.; Kazansky, V. B.; Beran, S.; Kubelkova, L.; Jiru, P. *J. Phys. Chem.* **1987**, *91*, 5247.

(21) Bates, S.; Dwyer, J. *J. Phys. Chem.* **1993**, *97*, 5897.

(22) Lunsford, J. H. Electron Spin Resonance Spectroscopy. In *Spectroscopy in Heterogeneous Catalysis*; Delgass W. N., Haller, G. L., Kellerman, R., Lunsford, J. H., Eds.; Academic Press: New York, 1979; p 183.

(23) Kasai, P. H.; Bishop, R. J. Electron Spin Resonance Studies of Zeolites. In *Zeolite Chemistry and Catalysis*; Rabo, J. A., Ed.; ACS Monograph 171; American Chemical Society, Washington, DC, 1976; p350.

(24) Lunsford, J. H. *J. Phys. Chem.* **1970**, *74*, 1518. Wang, K. M.; Lunsford, J. H. *J. Catal.* **1972**, *24*, 262. Lunsford, J. H.; Zingery, L. W.; Rosynek, M. P. *J. Catal.* **1975**, *38*, 179.

(25) Witzel, F.; Karge, H. G.; Gutsze, A. In *Proceedings of the 9th International Zeolite Conference, Montreal 1992*; von Ballmoos, R., Higgins, J. B., Treacy, M. M. J., Eds.; Butterworth-Heinemann: Woburn, MA, 1993; p 283.

(26) Gutsze, A.; Plato, M.; Karge, H. G.; Witzel, F. *J. Chem. Soc., Faraday Trans.* **1996**, *92*, 2495.

(27) Seidel, A.; Gutsze, A.; Boddenberg, B. *Chem. Phys. Lett.* **1997**, *275*, 113. Seidel, A.; Gutsze, A.; Boddenberg, B. In *Proceedings of the 12th International Zeolite Conference, Baltimore 1998*; Treacy, M. M. J., Marcus, B. K., Bisher, M. E., Higgins, J. B., Eds.; Warrendale, 1999; p 2589.

(28) Staudte, B.; Gutsze, A.; Bohlmann, W.; Pfeifer, H.; Pietrewicz, B. *Micropor. Mesopor. Mater.* **2000**, *40*, 1.

(29) Schoofs, B.; Schuermans, J.; Schoonheydt, R. A. *Microporous Mesoporous Mater.* **2000**, *35*−*36*, 99.

(30) Chang, C. D.; Chu, C. T.-W.; Miale, J. N.; Bridger, R. F.; Calvert, R. B. *J. Am. Chem. Soc.* **1984**, *106*, 8143.

(31) Weckhuysen, B. M., Van Der Voort, P., Catana, G., Eds. *Spectroscopy of Transition Metal Ions on Surfaces;* Leuven University Press: 2000.

(32) SIMPOW Simulation Program; Illinois EPR Research Center: Urbana-Champaign.

(33) Datka, J.; Gil, B.; Fraissard, J.; Massiani, P.; Batamack, P. In *Proceedings of the 12th International Zeolite Conference, Baltimore 1998*; Treacy, M. M. J., Marcus, B. K., Bisher, M. E., Higgins, J. B., Eds.; Warrendale, 1999; p 2595.

(34) Hadjiivanov, K. I. *Catal. Rev. Sci. Eng.* **2000**, *42*, 71.

(35) Anderson, M. W.; Klinowski, J.; Xinsheng, L. *J. Chem. Soc., Chem. Commun.* **1984**, 1596.

(36) Yamagishi, K.; Namba, S.; Yashima, T. *J. Catal.* **1990**, *121*, 47. Yamagishi, K.; Namba, S.; Yashima, T. *J. Phys. Chem.* **1991**, *95*, 872.

(37) Wu, P.; Komatsu, T.; Yashima, T. *J. Phys. Chem.* **1995**, *99*, 10923.

(38) Sulikowski, B.; Datka, J.; Gil, B.; Ptaszynski, J.; Klinowski, J. *J. Phys. Chem. B* **1997**, *101*, 6929.